On scaling properties of crossing the third-order resonance in particle accelerators

S.Y. Lee, X. Pang, Y. Jing, and T. Luo
Department of Physics, Indiana University, Bloomington, IN 47405, U.S.A.

K.Y. Ng
Fermilab, Batavia, IL 60510, US

We study effects of charged particle beams crossing a third-order resonance in an accelerator. The distortion of invariant torus during the resonance crossing is used to set 20% emittance growth or 2.5% of trap fraction as the cridtical resonance strength. We find a simple scaling law for the critical resonance strength vs the tune ramp rate and the initial emittance. The scaling law can be derived by solving Hamilton's equation of motion with *stationary phase condition*. Such scaling law can be used to evaluate the performance in high power accelerators, such as the FFAG and cyclotron.

PACS numbers: 29.27.Bd, 29.27.-a, 41.75.-i, 29.85.Fj

I. INTRODUCTION

Low order betatron resonances have been extensively studied in the design and operation of accelerators [1–4]. The third-order resonance plays a dominant role in dynamic aperture and may also limit accelerator performance. In particular, the betatron tunes of non-scaling Fixed-Field-Alternating-Gradient (FFAG) accelerators are designed to ramp through many resonances during the acceleration process. Careful studies of the scaling laws for the emittance growth during the passage of systematic space charge resonances are important [6–8].

Besides the systematic space charge resonances, low order random nonlinear resonance may also be important. This paper studies the scaling laws in crossing a non-space-charge-driven third-order resonance. This study may also help us improve the slow beam extraction in industrial and medical accelerators. The betatron tunes of an isochronous cyclotron may cross a few low order resonances during acceleration. Analysis of tolerable resonance is also important to the design and operation of cyclotrons.

There were recent detailed experiments at an FFAG accelerator on particle trapping efficiency of the third-order resonance islands [3]. These experiments are very important because a *non-scaling* FFAG accelerator may have to ramp through many third or other low order order resonances. Understanding the tolerance of these low order resonances are important in the design of future high power FFAG accelerators [9].

Earlier ambitious studies trying to derive a theoretical "trap fraction" during resonance crossing, have met some successes shown in Figs. 4 and 5 in Ref. [2]. However, the nonlinear equation of motion is difficult to solve, and the *criterion* that provides the trapping conditions needs experimental verification. Experimental data seems not able to fit well with the theoretical trap-fraction as shown in Fig. 15 of Ref. [3]. As indicated in Ref. [3] that the discrepancy may be due to imprecise modeling of the experimental condition. Nevertheless, numerical simulations agrees reasonably with the data.

When the betatron tune is ramped through a resonance, particles initially stream along the separatrix around resonance islands [1]. However, particles can not spontaneously jump into resonance islands. Trapping of particles in resonance islands requires the size of resonance islands to increase as the tune crosses the resonance and particles moving along the separatrix at an earlier time fall into the size-increasing islands. Such process may be difficult to put into a dynamic equation.

In this paper, we take a different path. Our aim is to derive a scaling law for a tolerable resonance strength in resonance crossing. We will solve Hamilton's equation of motion based on stationary phase condition. Our numerical simulation results, surprisingly, fit well with the scaling law.

We organize this paper as follows. Section II discusses our simulation model, where the accelerator lattice is made of 24 FODO cells with superperiodicity 24. Systematic octupoles are used to produce betatron detuning, and a single sextupole is used to generate an imperfect third-order resonance. Section III discusses the Hamiltonian, stable and unstable fixed points, separatrix, and phase space portraits near a third-order resonance. In Sec. IV, we examine the effect of phase distortion of a betatron phase space ellipse when a third order resonance ramp through the phase space. We characterize the phase space distortion via fractional emittance growth and the fraction of particle trapped into resonance islands. In Sec. V, we discuss the resonance crossing characteristics and scaling law for a Gaussian beam. We find that Hamilton's equation of motion may be used to explain the scaling properties of a Gaussian beam. Trapping of particles in resonance islands is discussed in Sec. VI, where we also compare our scaling law with that of Ref. [3]. The conclusion is given in Sec. VII.

II. THE MODEL

In our multi-particle simulation, we use an accelerator lattice with 24 FODO cells, where each FODO cell is composed of a focusing and a defocusing quadrupole with dipoles in between. The superperiodicity of our model lattice is $P = 24$ with betatron amplitude functions: $\beta_{x,F} = 40$ m, $\beta_{z,F} = 8.3$ m at the center of the focusing quadrupoles and $\beta_{x,D} = 6.3$ m, $\beta_{z,D} = 21.4$ m at the center of the defocusing quadrupoles. The horizontal betatron tune ramps downward from around 6.4 to 6.28 crossing a third-order resonance line at $\nu_x = 6 + \frac{1}{3}$ in various number of revolutions. The vertical tune is kept constant at all time. Octupoles are placed at all focusing quadrupole and defocusing quadrupole locations to provide nonlinear detuning. With 24 superperiods, these systematic octupoles do not drive resonance at the betatron tune of 6.25. A single sextupole is placed at one defocusing quadrupole location to create a random (or imperfection) sextupolar resonance, which occurs at $3\nu_x = \ell$ for $\ell =$ integer. On the other hand, a systematic resonance can only occur at $\ell = nP$, where n is an integer.

The initial transverse distribution of the beam is assumed to be bi-Gaussian cut-off at 6ϵ, where we use ϵ exclusively as the *statistical rms emittance* in this paper [10]. The maximum action of the initial distribution is 3ϵ. The transverse rms beam radii and emittances are calculated and updated at the end of each revolution. Detailed discussion of our simulation model has been discussed in Refs. [6, 7]. Our goal is to obtain a scaling law to be compared with that of Ref. [3], where space charge force was not included in simulations.

III. HAMILTONIAN AND THE FIXED POINTS

In our simulation model, particle motion can be described very well by a single resonance Hamiltonian near $3\nu = \ell$, in terms of action-angle variables [4, 10],

$$H = \nu J + \frac{1}{2}\alpha J^2 + GJ^{3/2}\cos(3\phi - \ell\theta + \xi) \qquad (1)$$

where J and ϕ are the conjugate action-angle variables for betatron oscillations, θ is the orbital angle serving as the independent "time coordinate", $\nu = \nu_x$ is the betatron tune, $\alpha = \alpha_{xx}$ is the nonlinear betatron detuning parameter arising from octupoles, the integer ℓ is 19 in our model, $G = |G_{30\ell}|$ is the resonance strength and ξ is the phase of $G_{30\ell}$ [10]. Equation (1) can be canonically transformed to

$$\tilde{H} = \delta I + \frac{1}{2}\alpha I^2 + GI^{3/2}\cos(3\psi) \qquad (2)$$

by the generating function $F_2 = (\phi - \frac{\ell}{3}\theta + \frac{\xi}{3})I$, where $I = J$ and $\psi = \phi - \frac{\ell}{3}\theta + \frac{\xi}{3}$ are the action-angle variables for the new Hamiltonian, $\delta = \nu - \frac{\ell}{3}$ is the proximity of the betatron tune to the resonance. Hereafter, we use either I or J symbol to represent the action in betatron motion, and may drop all trivial indices for simplicity.

The Hamilton's equations of motion are

$$\dot{I} = 3GI^{3/2}\sin(3\psi), \qquad (3)$$

$$\dot{\psi} = \delta + \alpha I + \frac{3}{2}GI^{1/2}\cos(3\psi), \qquad (4)$$

where the over-dot is the derivative with respect to the orbital angle θ. Fixed points (I_{fp}, ψ_{fp}) of the Hamiltonian are given by $\dot{I} = 0$ and $\dot{\psi} = 0$. For $\alpha > 0$ and $G > 0$, the quantity (I_{fp}, ψ_{fp}) are given by

- $\delta < 0$: UFP are $\psi_{fp} = 0, \pm 2\pi/3$ and

$$\frac{\alpha I_{fp}^{1/2}}{|G|} = -\frac{3}{4} + \frac{3}{4}\sqrt{1 - \frac{16\alpha\delta}{9G^2}}$$

- $0 \le \delta \le 9G^2/16\alpha$: UFP are $\psi_{fp} = \pi, \pm\pi/3$ and

$$\frac{\alpha I_{fp}^{1/2}}{|G|} = +\frac{3}{4} - \frac{3}{4}\sqrt{1 - \frac{16\alpha\delta}{9G^2}}$$

- $\delta \le 9G^2/16\alpha$: SFP are $\psi_{fp} = \pi, \pm\pi/3$ and

$$\frac{\alpha I_{fp}^{1/2}}{|G|} = +\frac{3}{4} + \frac{3}{4}\sqrt{1 - \frac{16\alpha\delta}{9G^2}}$$

For $\alpha > 0$ and $G < 0$, the J_{fp} listed above is still correct, except the phase angle ψ_{fp} increases by π. The bottom plot of Fig. 1 shows the stable and unstable fixed points for $\alpha > 0$. With $\alpha > 0$, fixed points exist when $\delta < \frac{9G^2}{16\alpha}$, where $\delta_{bif} = 9G^2/(16\alpha)$ is called the bifurcation tune. For $\alpha < 0$, these fixed points has mirror reflection with respect to the line $\delta = 0$ shown at the top plot of Fig. 1.

The unstable motion near the UFP is given by

$$\frac{d^2\Delta J}{d\theta^2} - 9|G|J_{ufp}^{1/2}\left(|\alpha|J_{ufp} + \frac{3}{4}|G|J_{ufp}^{1/2}\right)\Delta J = 0, \quad (5)$$

where $\Delta J = J - J_{ufp}$. The exponential growth rate at the UFP is proportional to $\sqrt{G}$, for small G.

Note that J_{sfp} is always larger than J_{ufp} with $\sqrt{J_{sfp}} - \sqrt{J_{ufp}} = |\frac{3G}{2\alpha}|$ for $\delta < 0$. The radial distance between the stable and unstable fixed points in the normalized phase space coordinates is $\sqrt{2\beta_x}|3G/2\alpha|$. The separatrix of the Hamiltonian is the torus that passes through the UFP. For the third-order resonance, the separatrix is given by

$$\delta J + \frac{1}{2}\alpha J^2 + GJ^{3/2}\cos 3\psi = \frac{1}{3}\delta J_{ufp} - \frac{1}{6}\alpha J_{ufp}^2. \quad (6)$$

Phase space portraits, including separatrices, across a third-order resonance have been shown in Fig. 12 of Ref. [3]. The separatrix in action-angle coordinates is shown in Fig. 2. The right plot shows the phase space

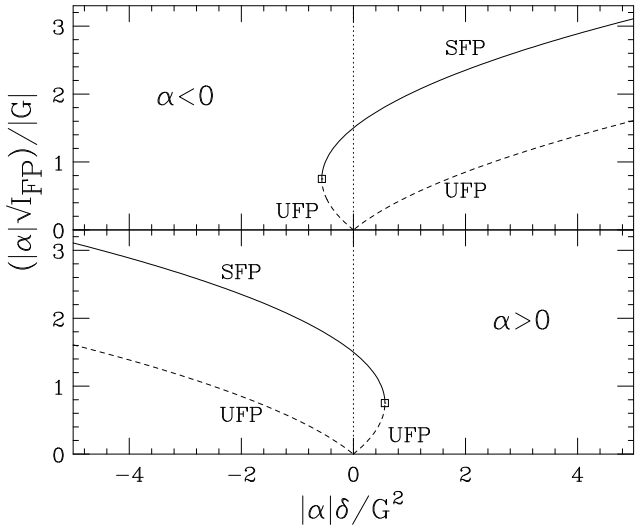

FIG. 1: The fixed points $|\alpha|I_{fp}^{1/2}/|G|$ vs $|\alpha|\delta/G^2$ for $\alpha < 0$ (top) and $\alpha > 0$ (bottom). The Stable and unstable FPs are shown as solid and dashed curves respectively. Bifurcation of the third-order resonance occurs at $\delta_{bif} = 9G^2/(16|\alpha|)$ marked by a rectangle.

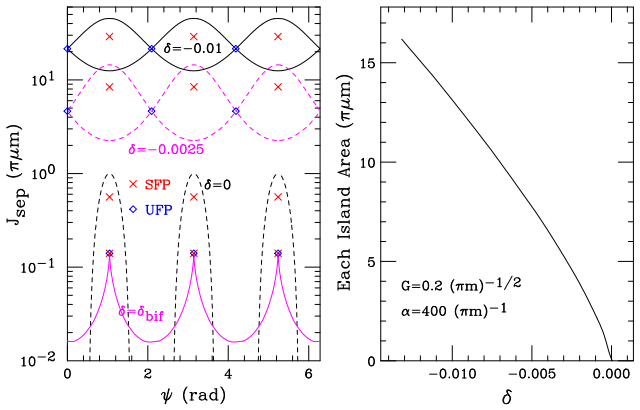

FIG. 2: Left: The separatrix for $\alpha = 400$ $(\pi\mathrm{m})^{-1}$, $G = 0.2$ $(\pi\mathrm{m})^{-1/2}$ for the proximity parameter $\delta = \delta_{bif}$, 0, and -0.0025, and -0.01 are drawn in action-angle variables in semi-log plot. SFPs are marked by X in red, and UFPs are marked diamond symbol in blue. The island size increases as the proximity parameter becomes smaller. Note that the vertical axis is in log scale. Right: the phase space of area of each resonance island vs the resonance proximity parameter δ. The phase space area of resonance island is found to scale with $G^{1/2}\alpha^{-5/4}$.

area of one island vs the resonance proximity parameter. As δ becomes more negative, the phase space area of resonance island increases.

It is difficult to find an analytic formula for the area of the resonance islands. However, the island area in the asymptotic region: $|\delta| \gg G^2/\alpha$, where $J_{ufp} \sim J_{sfp} \approx \left|\frac{\delta}{\alpha}\right|$, can easily be obtained from Eq. (6) to be

$$\text{Area} = \frac{16}{\pi}\,|G|^{1/2}|\delta|^{3/4}|\alpha|^{-5/4}. \qquad (7)$$

The area of the island for all cases can be numerically integrated along the separatrix, shown in the right plot of Fig. 2. The total island area (3 islands) indeed obeys a simple scaling property shown in Fig. 3, where the phase space area multiply the factor $G^{-1/2}\alpha^{+5/4}$ is plotted vs the resonance proximity parameter for a number of resonance strengths and detuning parameters. Equation (7) is drawn as a dashed curve for comparison. At a given α and G, the effect of the third-order resonance becomes more important for a beam with a larger emittance because the beam covers a larger action shown in the left plot of Fig. 2.

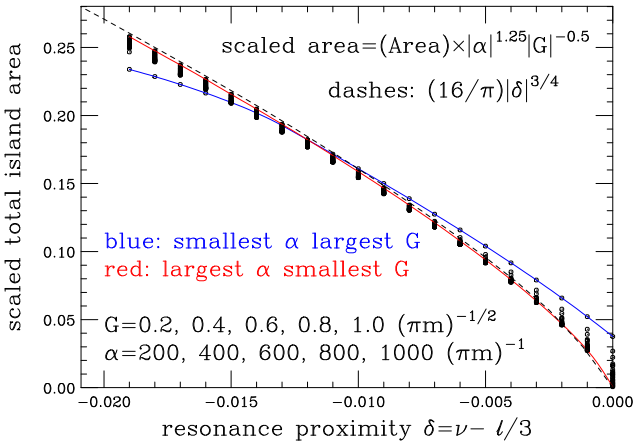

FIG. 3: The total phase space of 3 resonance islands multiplying the factor $G^{-1/2}\alpha^{5/4}$ vs the resonance proximity parameter δ for 25 cases. The phase space area of resonance island is found to scale with $G^{+1/2}\alpha^{-5/4}$. Eq. (7) based on the asymptotic approximation is shown in dashes for comparison. When α is large and G is small, the island area can be approximated by asymptotic limit shown as the red curve. When α is small and G is large, the phase space area deviates more from the asymptotic limit shown as the blue curve.

Based on Hamilton's equation (4), the stationary phase condition can occur around $\delta \sim \alpha\epsilon \sim |G|\sqrt{\epsilon}$, where ϵ is the rms beam emittance, which is defined as the rms phase space area of the beam. Experimental measurement of the third-order resonance shows that $|G_{30\ell}| \sim 1$ $(\pi\mathrm{m})^{-1/2}$ is a strong resonance. Using a pencil beam, we measured $G = 2.2$ $(\pi\mathrm{m})^{-1/2}$ at the IUCF Cooler [4]. Typical strengths of the 3rd order random resonances for FFAG accelerator designs [5] are about 0.01 to 0.5 $(\pi\mathrm{m})^{-1/2}$. The effective resonance strength is $G_{30\ell}\sqrt{\epsilon}$. Accelerators and storage rings are designed to have typically $\alpha \sim 10 - 1000$ $(\pi\mathrm{m})^{-1}$. Its effect on tune spread of the beam is $\alpha\epsilon$.

When the tune of an accelerator is slowly changing, the Hamiltonian is quasi-adiabatic. If there were no resonance, the action of each particle and the emittance of

the beam would be constant. However, when a resonance exists, the action of each particle will be perturbed. The fixed points and resonance islands are time dependent. Particle motion will still follow the quasi-static resonance dynamics moving along the separatrix.

We consider a beam with $6\epsilon = 30\ \pi\mu$m in an accelerator with $\alpha = 400\ (\pi\text{m})^{-1}$ encountering a third-order resonance with $G = 0.2\ (\pi\text{m})^{-1/2}$. The bifurcation tune of this resonance is $\delta_{bif} = 5.625 \times 10^{-5}$. If the bare betatron tune is ramped downward to $\nu = 6 + \frac{1}{3} + \delta_{bif}$, the SFP and UFP will appear for particles at action $J = 0.14\ \pi\mu$m, near center of the beam. The separatrix is shown as a curve with magenta color in Fig. 2. When the bare tune reaches $\nu = 6 + \frac{1}{3}$ or $\delta = 0$, we find $J_{ufp} = 0$ and $J_{sfp} \approx 0.56\ \pi\mu$m. The separatrix is marked as the dashed curve in black color. When the betatron tune reaches $\nu = 6 + \frac{1}{3} - 0.0025$, we find the $J_{ufp} \approx 4.7\ \pi\mu$m and $J_{sfp} = 8.5\ \pi\mu$m. The dashed magenta colored curve in Fig. 2 is the separatrix. These resonance islands inside the beam emittance move outward as the betatron tune continues to move downward.

Now, we consider the case of an upward ramping betatron tune. When the bare betatron tune reaches $\nu = 6 + \frac{1}{3} - 0.01$, we find $J_{ufp} = 21\ \pi\mu$m and $J_{sfp} = 29\ \pi\mu$m. Particle actions larger than 12 $\pi\mu$m are strongly perturbed as shown in the separatrix on Fig. 2. Particles stream along the separatrix to larger actions. When the betatron tune reaches $\nu = 6 + \frac{1}{3} - 0.0025$, we have $J_{ufp} \approx 4.7\ \pi\mu$m and $J_{sfp} = 8.5\ \pi\mu$m. The separatrix is marked as a dashed magenta colored curve on Fig. 2 and the size of resonance islands becomes smaller. When the bare tune reaches $\nu = 6 + \frac{1}{3}$, we have $J_{ufp} = 0$ and $J_{sfp} \approx 0.56\ \pi\mu$m. The separatrix is marked as dashed curve with black color. When $\nu = 6 + \frac{1}{3} + \delta_{bif}$, the SFP and UFP are located at action $J = 0.14\ \pi\mu$m. They disappear together as the tune moves further upward.

Without loss of generality, we consider in the rest of the paper the ramping of tune from a higher value to a lower value crossing a third-order resonance, i.e. δ changes from positive to negative in Fig. 1. The scenarios with $\alpha > 0$ or $\alpha < 0$ cases are demonstrated as follows.

A. The case with $\alpha > 0$

If $|G|$ is not very large, the bifurcation action $\frac{9}{16}(G/\alpha)^2$ is less than the phase space area. The resonance will create empty islands inside the bunch phase space. Particle motion will stream along the separatrices. As the betatron tune is further lowered to $\delta = 0$, the UFP moves inward to the $J_{ufp} = 0$ and SFP moves outward to $J_{sfp} = \frac{9}{4}(G/\alpha)^2$, as shown in Figs. 1 and 2. When the betatron tune moves past $\delta < 0$, both the UFP and SFP move outward and the size of resonance islands increases, and some particles will be trapped in resonance islands. These trapped particles will be carried outward in phase space as the tune is further lowered.

We demonstrate this effect in multi-particle simulation shown in Fig. 4. Particles are driven out of the center by the resonance and may be captured into resonance islands. The resonance first starts near the center of the beam, particles are driven out along the separatrix, and later captured and trapped by the ever increasing islands. These islands keep moving outward with the SFPs until the aperture limit is reached. The continuous growth of the SFPs accounts for the linear increase of the horizontal emittance in the bottom left plot of Fig. 5. In this case, particles trapped in the resonance islands around the SFPs will eventually be lost.

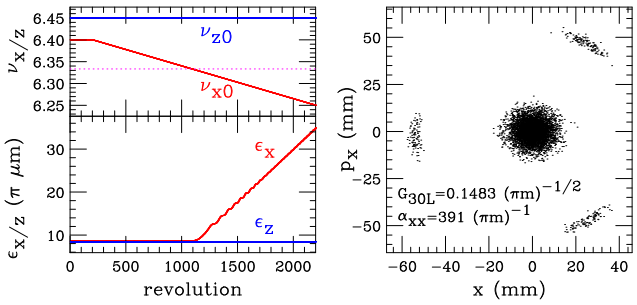

FIG. 4: (Color) Top-left: Horizontal bare betatron tune is ramped downwards from $(\nu_x, \nu_z) = (6.40, 6.45)$ starting from turn 200 to $(6.25, 6.45)$ at turn 2200 (ramp rate -0.000075 per turn) through a third-order resonance $3\nu_x = 19$ at turn 1100. Bottom-left: Red and blue curves are respectively the horizontal and vertical emittances. Horizontal emittance grows when the resonance is crossed. Right: Horizontal phase-space distribution at turn 2200 shows 3 resonance islands. The detuning parameter is $\alpha > 0$.

B. The case with $\alpha < 0$

For $\alpha < 0$, the fixed points move inward as shown in the top plot of Fig. 1 when the tune is ramped from a higher value to a lower value. large amplitude particles see the resonance first, and the resonance The resonance islands encroach the beam phase space and drive particle outward along the separatrices. These particles move along the separatrix, and cause emittance growth. How much emittance growth depends on how long the beam stays near the resonance and how strong the resonance is.

As the tune is further lowered, the islands move inward and get smaller in size, until the point of bifurcation. No particle will be trapped into resonance islands, but emittance of the beam will increase. Unlike the $\alpha > 0$ case, these escaping particles are not captured by the SFPs due to the decreasing size of resonance islands. Instead, they spiral along the separatrix and the emittance becomes larger. When δ becomes negative and less than δ_{bif}, the resonance disappears. Figure 5 shows the simulation of 5000 particles ramping through a third-order resonance with $\alpha < 0$. Note that the emittance begins to increase before the bare tune reaches the third-order resonance.

After the resonance is crossed, the emittance becomes constant because no particle is trapped into resonance islands.

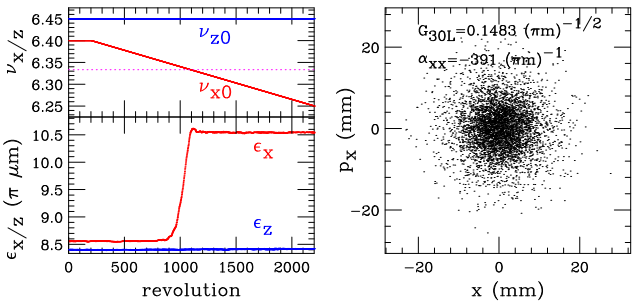

FIG. 5: (Color) Top-left: Horizontal bare betatron tune is ramped downwards from $(\nu_x, \nu_z) = (6.40, 6.45)$ starting from turn 200 to $(6.25, 6.45)$ at turn 2200 (ramp rate -0.000075 per turn), where the third-order resonances $3\nu_x = 19$ is crossed at turn 1100. Bottom-left: Red and blue curves are respectively the horizontal and vertical emittances. Horizontal emittance increases before the bare tune crosses the resonance. Right: Horizontal phase-space distribution at turn 2200 shows no particle being trapped in resonance islands. Here the detuning parameter $\alpha < 0$.

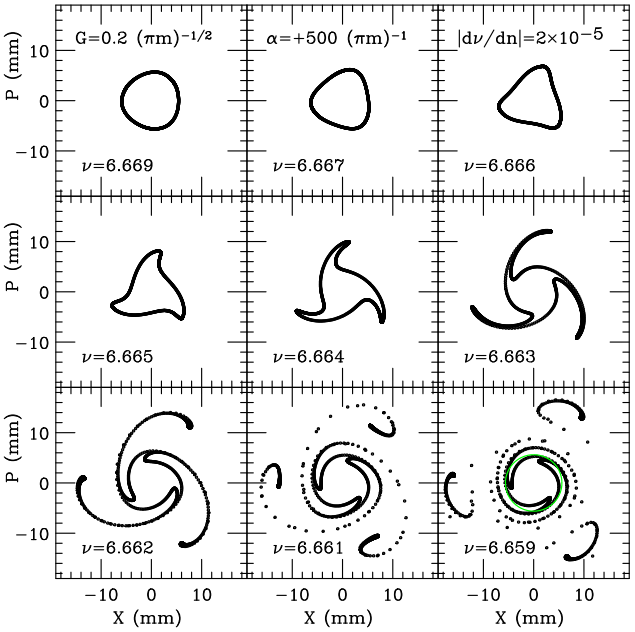

FIG. 6: (Color) The time lapse of the Poincaré maps of a ring-beam during the passage of a third order resonance crossing for the case of $\alpha = \alpha_{xx} > 0$. Note that particles moves along the separatrices and are captured into resonance islands, which carry the captured particles outward. The Green curve at the bottom-right plot is the initial beam distribution.

IV. RESONANCE CROSSING OF A RING-BEAM

In this section, we study emittance growth of a ring-beam in resonance crossing. We consider a beam which consisting of particles uniformly distributed on a ring in phase space with a constant action J. The rms emittance of the ring-beam is $\epsilon_i = J$ [10].

When the betatron tune is ramping downward at a rate of $|d\nu/dn|$ crossing a third order resonance, the phase space ellipse will be distorted. Particles will move along the separatrices and possibly captured by the resonance islands. Figures 6 and 7 shows the time-lapsed Poincaré maps during the resonance crossing.

For $\alpha < 0$, it is easy to characterize the emittance growth by defining the fractional emittance growth (FEG) as

$$\text{FEG} = \frac{\Delta\epsilon}{\epsilon_i}, \tag{8}$$

where ϵ_i is the initial emittance. For $\alpha > 0$, the beam emittance continues to grow as trapped particles being transported outward in the resonance islands. We can characterize the effect of resonance as the fraction of particles being trapped in resonance islands, i.e.

$$\text{Trap Fraction} = \frac{\text{Number of particles in islands}}{\text{Total number of particles}} \tag{9}$$

Figure 8 shows the FEG and trap-fraction exhibit oscillation vs the tune ramp rate. This oscillation reveals the complex dynamics of particle motion along the separatrices. As particles moves along the separatrices, particles are folded into slices. When particles accumulated near the separatrix are resides at the outer part of the resonance island at the time the resonance crosses the ellipse, the FEG will be large. On the other hand, if these particles move to the inner section of the island at the time resonance moves away, the FEG becomes small. The oscillatory structure in Fig. 8 reflects the dependence of the island tune vs resonance parameters.

We first consider the case with $\alpha < 0$. Figure 9 shows the FEG vs the ramp rate for different detuning α. The FEG is nearly independent of α at fast resonance crossing rates. However, at adiabatic slow crossing rates, the limiting values of the FEG do depend on α.

We examine the physics of the adiabatic FEG limit. Figure 10 shows the time lapse of particle motion when the resonance is slowly crossing the phase space ellipse. The time lapse phase portraits reveal the emittance growth mechanism. As the resonance reaches the ellipse, the phase space is adiabatically deformed to the inner ellipse, and as the resonance moves away, particle will distributed along the outer orbit of the separatrices. The FEG is the ratio of the island-area divided by the initial phase area, which is equal to the are of the inner area bounded by the separatrices shown in the top 4 plots of Fig. 10. After the resonance moves away, the phase space ellipse follows the Hamiltonian torus and the phase space area does not change.

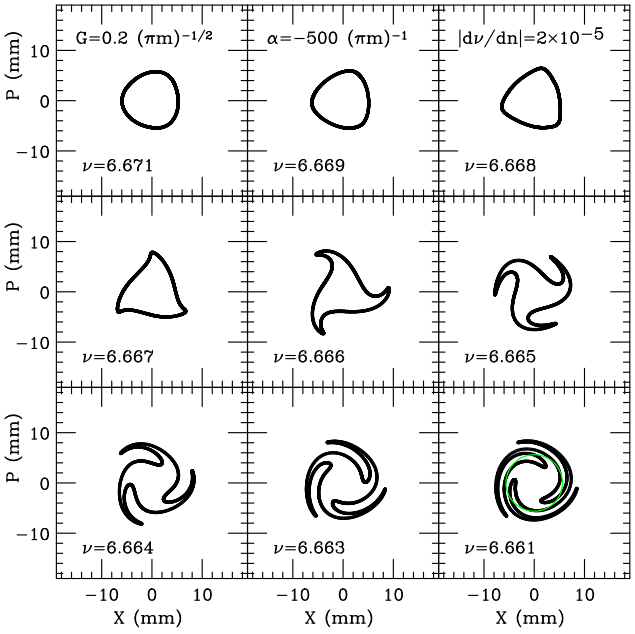

FIG. 7: (Color) The evolution of a ring-beam during the passage of a third resonance crossing the beam ellipse for the case of $\alpha = \alpha_{xx} < 0$. The phase space ellipse is distorted, squeezed out along the separatrix, and left distorted as the resonance moving inward after crossing the ellipse. The Green curve at the bottom-right plot is the initial beam distribution.

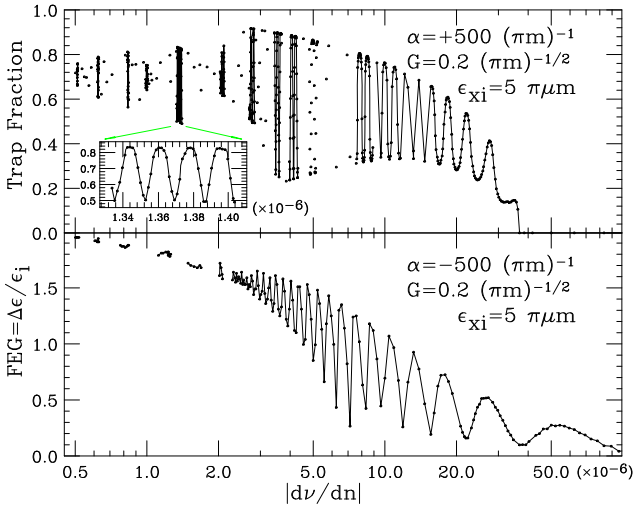

FIG. 8: (Color) Top: Trap Fraction vs tune ramp rate for $\alpha > 0$. Bottom: FEG vs tune ramp rate for $\alpha < 0$. Both cases have $\epsilon_i = 2.5\pi\mu$m and $G = 0.2$ $(\pi\text{m})^{-1/2}$. The oscillating nature of these quantities reveals dynamics of particle motion along the separatrices as the resonance passes through the phase ellipse of the beam.

We calculate the island-area of the resonance Hamiltonian at the instant that the inner stable area is equal to initial phase space ellipse to compare with numerically obtained FEG. Figure 11 compares the simulation result with theory (in green), i.e. $\Delta\epsilon \approx 7.3G\sqrt{\epsilon}/\alpha$. The adiabatic condition can be used to calculate the fractional emittance growth for an arbitrary initial beam distribution. For example, if the initial beam distribution is $\rho(J)$ with $\int \rho(J) = 1$ and $\epsilon_{\rm rms} = \int J\rho(J)dJ$. The resulting fractional emittance growth becomes

$$\text{FEG} = 7.3 \int \frac{G\sqrt{J}}{\alpha}\rho(J)dJ. \qquad (10)$$

For a Gaussian beam, the adiabatic fractional emittance growth is $7.3\Gamma(3/2)G/(|\alpha|\sqrt{\epsilon_{\rm rms}})$, where Γ is the Gamma Function.

The trap-fraction shows oscillatory structure even at a very slow tune ramp rate. as shown in Fig. 8. Even at a very slow ramping rate of about $|d\nu/dn| = 4 \times 10^{-7}$, the trap fraction vs the resonance strength, see Fig. 12, shows oscillatory structure. As the resonance islands pass through phase-space region of the beam, particles are grouped together at resonance UFPs. If this group of high density particles happen to be in the phase space region that resonance islands move through, they will be captured into resonance islands and the trap-fraction will be high. On the other hand, if the high density group happens to be outside of the resonance island bucket, the trap-fraction will be low. The beam can be fully captured

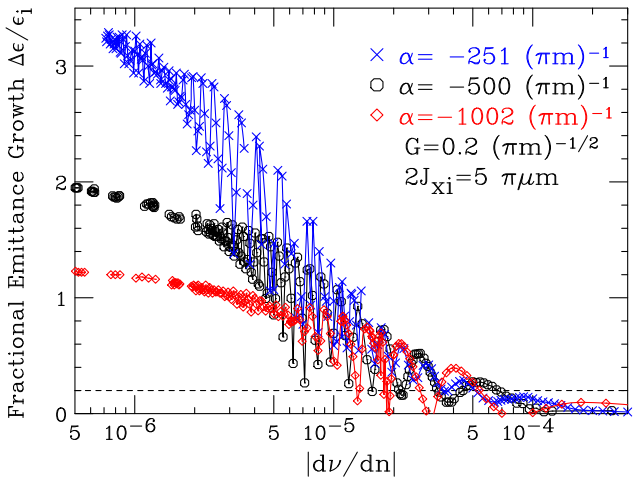

FIG. 9: (Color) The FEG vs the tune ramp rate. Note that the FEGs reach limits which depend on the detuning parameter at small tune ramp rate. The FEG is nearly independent of α at a large tune ramp rate. The oscillating structure depends on details of particle motion along the separatrices.

only when the resonance strength is large. The capture rate depends on the dynamics when the particles, moving along the separatrices, fall into the enlarging resonance islands as the tune ramps through the phase space ellipse of the beam.

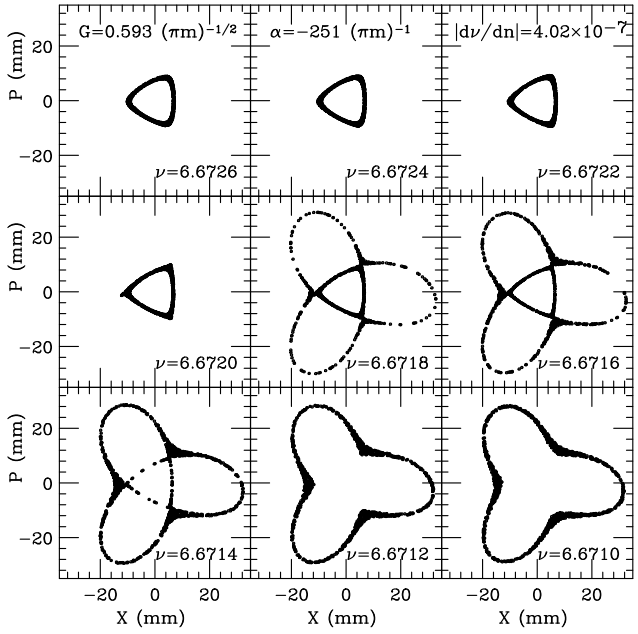

FIG. 10: (Color) The time-lapse Poincaré maps as the 3rd order resonance crosses the phase space ellipse at an adiabatic (slow) crossing rate. The FEG is equal to the ratio of the area of outer resonance islands divided by the inner stable area, which is equal to the initial phase space area of the original ellipse.

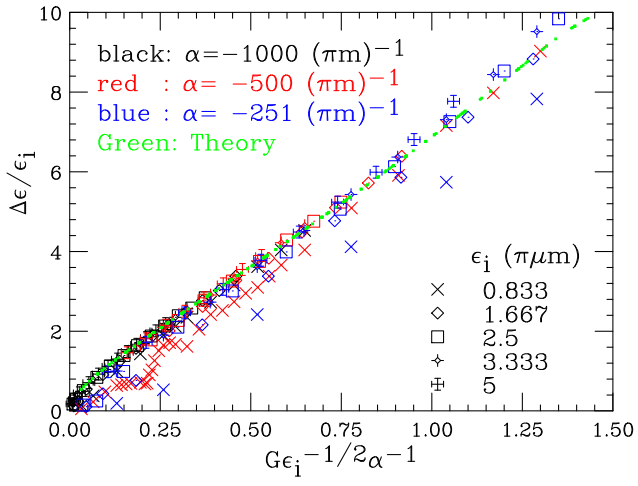

FIG. 11: (Color) The FEG obtained by multi-particle simulation is compared with theory. Note that the FEG depends nearly linearly with respect to $G\sqrt{\epsilon_i}/\alpha$.

V. RESONANCE CROSSING OF A GAUSSIAN BEAM

In FFAG accelerators, betatron tunes ramp through many resonances. The tune ramp rate depends on energy gain per turn. The adiabatic fraction emittance growth of Eq. (10) is too large. One tries to ramp through the resonances as fast as possible. Typical tune ramp rate is about $10^{-3} \sim 10^{-5}$ per revolution.

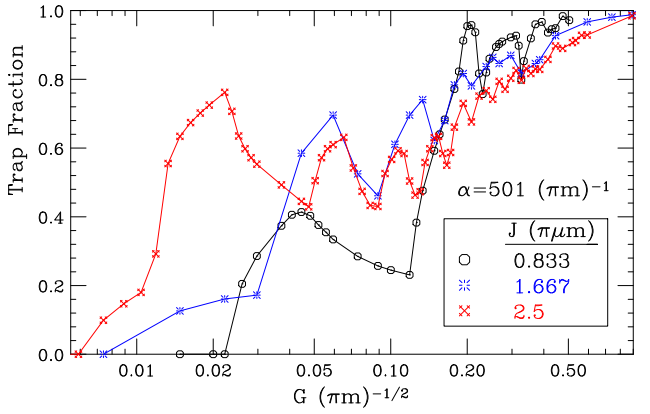

FIG. 12: (Color) Trap fraction vs resonance strength for different initial actions of the ring beam. The detuning parameter is 501 $(\pi\mathrm{m})^{-1}$. Note that the resonance can not trap particle only when the resonance strength is very small!

Since the effects of resonance crossing are markedly different for the $\alpha < 0$ case, we define the emittance growth factor (EGF) as

$$\mathrm{EGF} = \frac{\epsilon_{\mathrm{final}}}{\epsilon_{\mathrm{initial}}} = 1 + FEG \tag{11}$$

to quantify the effect of resonance crossing. Here $\epsilon_{\mathrm{final}}$ is the final emittance after passing through the resonance, and $\epsilon_{\mathrm{initial}}$ is the initial beam emittance. On the other hand, the trap fraction defined in Eq. (9) is difficult to quantify for $\alpha > 0$. Furthermore, particles being excited outside the original phase space area can be as dangerous as particles trapped in resonance islands. Thus it is more logical to define the quantity f_{trap} as:

$$f_{\mathrm{trap}} = \frac{N_{J>J_{i,max}}}{N_{\mathrm{total}}}, \tag{12}$$

to quantify the effects of resonance crossing. Here, N_{total} is the total number of particles in our tracking, and $N_{J>J_{i,max}}$ is the number of particles with action J larger than that of maximum initial maximum action after passing through the resonance. We choose $J_{i,max} = 3\epsilon_{\mathrm{initial}}$ in our initial beam distribution. Typically, we use about 5000 particles in multi-particle tracking. Note that our definition of trapping efficiency differs from Eq. (9), which may also differ from that of Ref. [2]. Our definition of f_{trap} includes particles move along separatrices and become lost. Nevertheless, our definition should agree better with experiments using scraping method to remove large amplitude particles.

For the negative α case, no particle will be trapped in resonance islands after the resonance crossing. We can use both EGF and f_{trap} to characterize the resonance crossing. Although there is no particle trapped in resonance islands, particles excited outside the initial beam emittance is considered to be perturbed by resonance crossing. We characterize the relation between

EGF and $f_{\rm trap}$. The EGF of a Gaussian beam is an ensemble average of the ring-beam with different actions shown in Fig. 9. Figure 13 shows the relation between EGF and $f_{\rm trap}$. Since more particles being driven out of original maximum action will produce a higher emittance growth, the correlation between the EGF and $f_{\rm trap}$ is evident. A 20% emittance growth is equivalent to 2.5% of particles being driven outside the maximum initial action. Although, the EGF has no meaning for $\alpha > 0$, the quantity $f_{\rm trap}$ is well defined and the prescription of $f_{\rm trap} = 2.5\%$ is applicable.

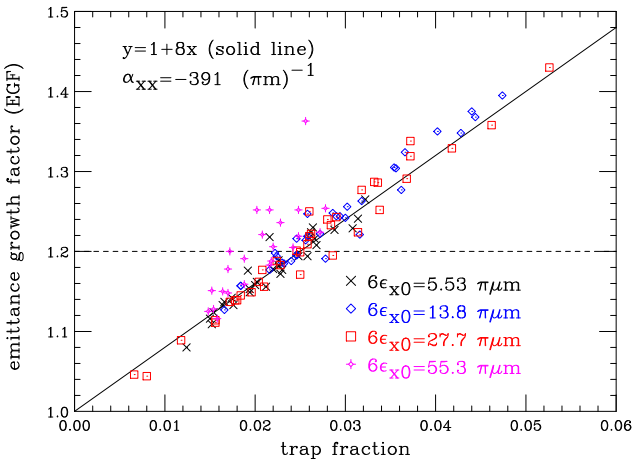

FIG. 13: (Color) The correlation between EGF and $f_{\rm trap}$ for $\alpha < 0$ for beams with different emittances (different colors). It appears that the ensemble average has washed out oscillatory structure of Fig. 9. For each emittance, the resonance strength $|G_{30\ell}|$ varies from 0.07 to 1.2 $(\pi{\rm m})^{-1/2}$ and the crossing speed varies from 1.2×10^{-3} to 2×10^{-5} per turn.

A. Resonance crossing with $\alpha < 0$

We consider three cases with $|G_{30\ell}| = 0.86$, 0.44, and 0.15 $(\pi{\rm m})^{-1/2}$. Figure 14 shows the EGF−1 or $\Delta\epsilon/\epsilon$ vs the tune ramp rate for the case with a large detuning parameter $\alpha = -783$ $(\pi{\rm m})^{-1}$ and rms emittance $\epsilon_{x0} = 4.62$ π-μm. The initial distribution cut-off action is $2J_{i,max} = 6\epsilon_{x0}$ in bi-Gaussian distribution. We find that the scaling dependence varies from $|d\nu/dn|^{-1/2}$ to $|d\nu/dn|^{-2/3}$. A larger resonance strength reaches saturation earlier and at a high EGF, in agreement with the scaling of the area of resonance islands. The first regime with EGF−1 ≤ 0.2, the growth of EGF obeys the scaling law of $|d\nu/dn|^{-1/2}$ (shown as dash-dotted curve to guide our eyes), while a larger EGF follows the scaling law of $|d\nu/dn|^{-2/3}$ (shown as dashed line).

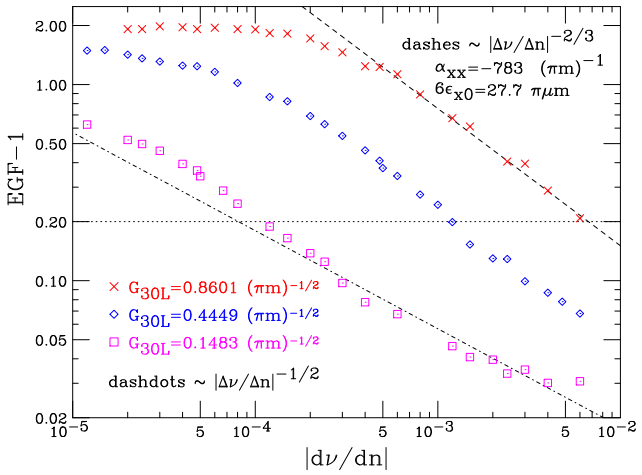

FIG. 14: (Color) The EGF−1 for large, medium, and small resonance strengths are shown for comparison. At very slow tune ramp rate, the EGF reaches a saturation. The saturated value is proportional to the third-order resonance island height, and thus proportional to $\sqrt{|G_{30\ell}|}$ for the large detuning cases.

B. Initial Growth Mechanism

When the resonance crossing rate is reasonably high, particles will stream along the separatrix without reaching adiabatic limit of Figs. 6 and 7. The increase of action is most influenced by the stationary phase condition of Eq. (3). The change of action is

$$\Delta J = \langle 3GJ^{3/2}\sin 3\psi_{sp}\rangle[2\pi(\Delta n)_{sp}], \qquad (13)$$

where $\langle\cdots\rangle$ is the ensemble average of the beam distribution during the time the resonance separatrices reach the beam phase space region, $(\Delta n)_{sp}$ is the number of revolutions that the resonance phase remains stationary. The evolution of phase obeys Eq. (4). At resonance with stationary phase, we find $\dot\psi_{sp} \approx 0$ (but ψ_{sp} is not necessary 0), and its "time" derivative is

$$\ddot\psi = \dot\delta = \frac{1}{2\pi}\frac{d\nu}{dn}, \qquad (14)$$

where $(d\nu/dn)$ is the tune change per revolution. For a constant ramping through a resonance, we find

$$\Delta\psi \approx \frac{1}{4\pi}\left|\frac{d\nu}{dn}\right|(2\pi\Delta n)^2. \qquad (15)$$

The number of turn in stationary phase condition is

$$\Delta n_{sp} \approx \left(\frac{\Delta\psi_{sp}}{\pi\left|\frac{d\nu}{dn}\right|}\right)^{1/2} \qquad (16)$$

The maximum change of action is obtained by substituting $2J = 6\epsilon_{x0}$. Identifying the largest change of action

as $\Delta\epsilon$, we find

$$\frac{\Delta\epsilon}{\epsilon} \approx G\sqrt{\epsilon}\left|\frac{d\nu}{dn}\right|^{-1/2}\left\{6\sqrt{3\pi}\langle\sin 3\psi_{sp}\rangle(\Delta\psi_{sp})^{1/2}\right\}. \tag{17}$$

The initial phase of emittance growth should obey the scaling property:

$$\frac{\Delta\epsilon}{\epsilon^{3/2}}\left|\frac{d\nu}{dn}\right|^{1/2} \approx FG \tag{18}$$

where the constant is $F \approx 6\sqrt{3\pi}\langle\sin\psi_{sp}\rangle\,(\Delta\psi_{sp})^{1/2}$. As shown in Figs. 6 and 7, the initial growth is to squeeze particles from the inner parts of the separatrices toward the outer parts of the separatrices, and $\langle\sin 3\psi_{sp}\rangle$ always positive. A simple estimation with $\langle\sin 3\psi_{sp}\rangle \approx \frac{1}{2}$ and $\Delta\psi_{sp} \approx \frac{1}{4}$ gives $F \approx 5$. The initial growth is independent of the detuning parameter! The left plot of Fig. 15 shows the emittance growth vs revolution number for various detuning parameters. When the tune ramp rate is not too small as shown in Fig. 9, the emittance growth is nearly independent of the detuning parameter α in accordance of Eq. (18). One can understand the result as follows. When α is small, the island size is larger, and some particles will be excited to a larger phase space positions. On the other hand, a large α will have a smaller island size, but many more particles are driven out of the core. The resulting rms emittances are about the same.

The right plot of Fig. 15 shows a compilation of simulation data: $\frac{\Delta\epsilon}{\epsilon^{3/2}}\left|\frac{d\nu}{dn}\right|^{1/2}$ vs the resonance strength G. The simulation data are compiled with simulations with various parameters: α from 0 to -800 $(\pi\mathrm{m})^{-1}$, $G_{30\ell}$ from 0.02 to 0.8 $(\pi\mathrm{m})^{-1/2}$, $|d\nu/dn|$ from 10^{-5} to 10^{-2}, and the rms emittances from 0.93, 2.3, 4.62, 6.94, and 9.26 $\pi\mu$m. A line (red) $7\times G_{30\ell}+8\times G_{30\ell}^2$ is drawn through data to guide our eyes. The part that depends linearly on G is to be compared with the constant F in Eq. (18). The spread of the simulation result reflects the oscillatory structure of Fig. 9. The deviation from the stationary phase condition can be important.

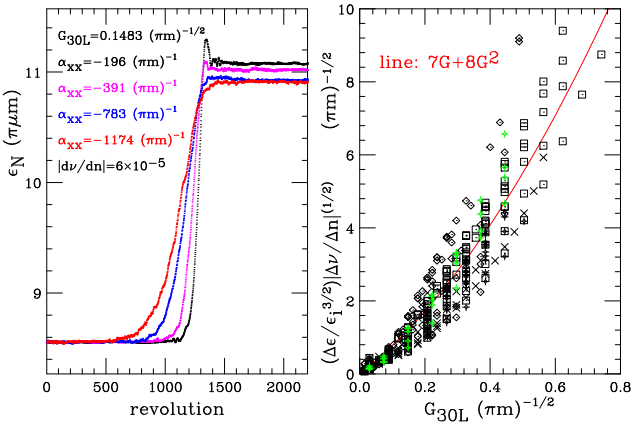

FIG. 15: (Color) Left: emittance growth in passing through a third-order resonance at a tune ramp rate of $|d\nu/dn| = 6\times 10^{-5}$, $G = 0.1483$ $(\pi\mathrm{m})^{-1/2}$ for various detuning parameters. Right: $\frac{\Delta\epsilon}{\epsilon^{3/2}}\left|\frac{d\nu}{dn}\right|^{1/2}$ derived from simulation data is plotted vs G. The initial emittance is $\epsilon = 4.62$ $\pi\mu$m. The simulation data are compiled with simulations with various parameters: α from 0 to -800 $(\pi\mathrm{m})^{-1}$, $G_{30\ell}$ from 0.02 to 0.8 $(\pi\mathrm{m})^{-1/2}$, and $|d\nu/dn|$ from 10^{-5} to 10^{-2}. A red line $7G_{30\ell}+8G_{30\ell}^2$ is drawn through data to guide our eyes. The linear part is to compare with the constant F in Eq. (18). Because the large range of α and G, the resulting spread in the EGF is large. This spread also reflects the oscillatory nature of Figs. 8 and 9.

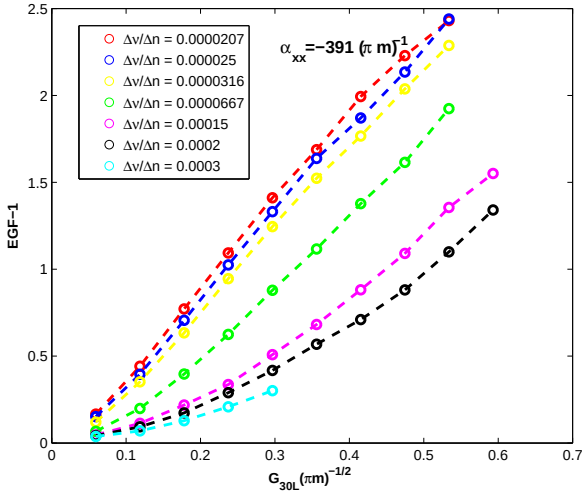

FIG. 16: (Color) With negative detuning coefficient $\alpha_{xx} = -391$ $(\pi\mathrm{m})^{-1}$, the emittance growth factor (EGF) increases with resonance strength $G_{30\ell}$. Faster ramping rate results in less emittance growth. Initial emittance is $\epsilon_{x,0} = 4.62\pi\mu m$.

C. Scaling law for the resonance strength

Our main task in this paper is to obtain a critical (tolerable) resonance strength when the betatron tune of a beam ramps through a third-order resonance. We define a critical resonance strength as the resonance strength for an emittance growth of 20% in passing through a resonance. Figure 16 shows the quantity EGF-1 for $\alpha = -391$ $(\pi\mathrm{m})^{-1}$ and $\epsilon = 4.62$ $\pi\mu$m as a function of the resonance strength $G_{30\ell}$ for different ramping rates.

A faster ramping rate has less emittance growth. A line at EGF=1.2 intercepts all the lines on Fig. 16 is used to define the critical resonance strength $\kappa_{30\ell}$, which is the resonance strength for a 20% emittance growth at a particular tune ramping rate. One can extract the critical resonance strength for different detuning parameters. Figure 17 shows a power law relationship between the critical resonance strength $\kappa_{30\ell}$ vs the betatron tune ramping rate for various detuning parameters. As indicated in Eq. (18), the initial emittance growth scales with $|\Delta\nu/\Delta n|^{0.5}$ shown as a dashed line to guide the eyes. The

critical resonance strength for 20% emittance growth is nearly independent of the betatron detuning parameter.

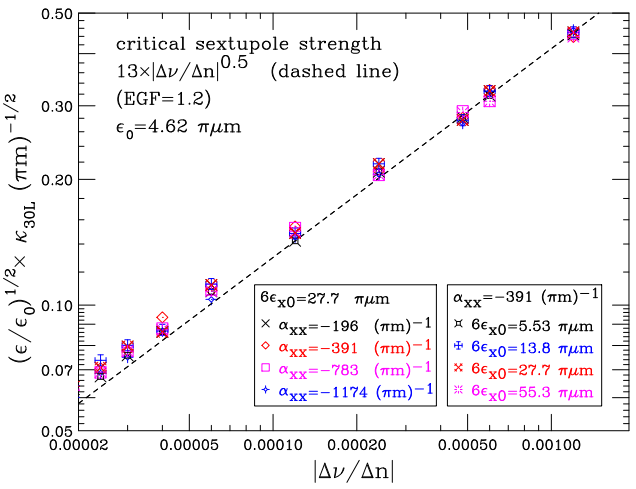

FIG. 17: (Color) The scaled critical resonance strength $\kappa_{30\ell}\sqrt{\epsilon/\epsilon_0}$ vs. tune ramping rate for various detuning coefficients and various initial emittances. The detuning coefficients are varied at a fixed initial emittance $\epsilon = 4.62\ \pi\mu$m. The emittance is then varied at a fixed detuning coefficient $\alpha_{xx} = -391\ (\pi\text{m})^{-1}$. The critical resonance strength is inversely scaled by the square root of the ratio of the initial emittance to the reference emittance of $\epsilon_0 = 4.62\pi\mu$m.

The emittance growth also depends on the initial beam emittance. The effective resonance strength for a beam crossing the third-order resonance is "$G\sqrt{\epsilon}$". Thus the critical resonance strength $\kappa_{30\ell}$ should scale inversely with $1/\sqrt{\epsilon}$. Figure 17 shows the scaled effective critical resonance strength, reference to that of the $\epsilon_0 = 4.62\ \pi\mu$m data.

Combining these two case shown in Fig. 17, we find the power law of the critical resonance strength is

$$\kappa_{30\ell} = 13\left\{\frac{4.62\ [\pi\mu\text{m}]}{\epsilon\ [\pi\mu\text{m}]}\right\}^{0.5}\left\{\left|\frac{\Delta\nu}{\Delta n}\right|\right\}^{0.5}\ [(\pi\text{m})^{-1/2}], \tag{19}$$

where ϵ is the initial rms emittance of the beam in the unit of $[\pi\mu\text{m}]$, and the reference emittance is $4.62\ \pi\mu$m shown in Fig. 17. The factor 13 in Eq. (19) agrees with Eq. (18) by setting the factor of $F \approx 7$ and $\Delta\epsilon/\epsilon = 0.2$. If we select all data of Fig. 15 that have EGF ~ 1.2. The resulting plot of $\frac{\Delta\epsilon}{\epsilon^{3/2}}\left|\frac{d\nu}{dn}\right|^{1/2}$ vs G is shown in Fig. 18. We find that $F \approx 7$ fits well with the data.

VI. TRAP OF PARTICLES IN RESONANCE ISLANDS

Although EGF is an indicator for a resonance in the negative detuning case, this indicator can not be used for the positive detuning cases. We have introduced the trap fraction defined as the fraction of particles kicked out of the original beam size. Figure 13 shows the relationship

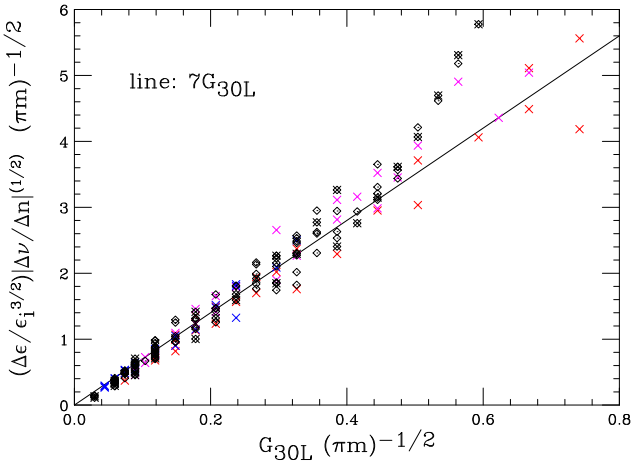

FIG. 18: (Color) $\frac{\Delta\epsilon}{\epsilon^{-3/2}}\left|\frac{d\nu}{dn}\right|^{1/2}$ vs G for data with EGF falls within 1.05 to about 1.3. For this set of data, the emittance growth dynamics can be described by Eq. (14).

between the EGF and the trap fraction. One observes that EGF=1.2 amounts to 2.5% of trap fraction. We thus define the *critical resonance strength* as 2.5% of particles being excited to have an action larger than the initial maximum action of the beam.

Figure 19 shows the trap fractions calculated for different ramping rates with octupole detuning parameter $\alpha_{xx} = 391\ (\pi\text{m})^{-1}$. Particles, driven outward by the third-order resonance and moved beyond a dynamic aperture, are also considered as trapped particles. Larger resonance strengths cause more particles to be pushed out of the center core and captured by the resonance islands. Data from Ref. [3] are also shown with blue and red boxes. It appears that the experimental data agree reasonably well with our simulation results with tune ramp rates 8.6×10^5 and 1.4×10^4 per turn.

Similar to the scaling property shown in Sec. V C, we define the equivalent resonance strength as

$$G^{eq}_{30\ell} = G_{30\ell}\left(\frac{\epsilon\ [\pi\mu\text{m}]}{4.62\ [\pi\mu\text{m}]}\right)^{1/2} \tag{20}$$

reference to the beam emittance of $6\epsilon = 27.7\ \pi\mu$m. Figure 20 shows the trap fraction vs the equivalent resonance strength for different emittances for a constant ramping rate of $d\nu/dn = 6\times10^{-5}$. Our results show that the equivalent resonance strength can be used to characterize the trap fraction. A line $f_{\text{trap}} \approx G^{\text{eq}}_{30\ell} - 0.07\ (\pi\text{m})^{1/2}$ drawn through data is to guide the eyes. The equivalent resonance strengths of Ref. [3] are 0.27, 0.19, 0.31 $(\pi\text{m})^{-1/2}$ with the tune ramp rates of 8.6×10^{-5} and 1.4×10^{-4}. We plot these data in Fig. 19 for comparison.

A. Scaling law for trap particles

For a given ramping rate, we define the critical resonance strength $\kappa_{30\ell}$ as the resonance strength that pro-

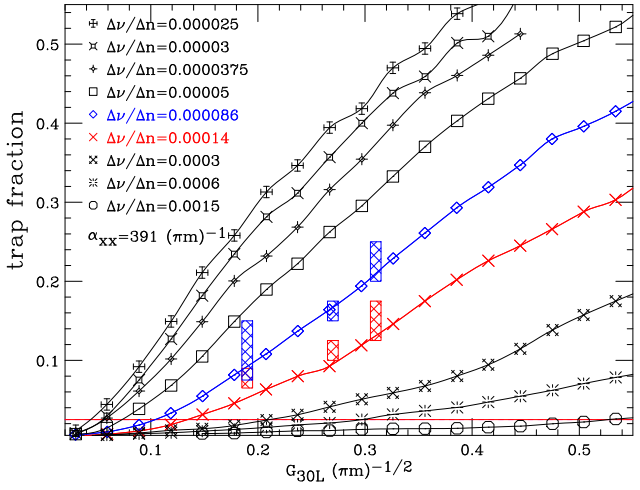

FIG. 19: (Color online) With positive detuning coefficient $\alpha_{xx} = 391(\pi\mathrm{m})^{-1}$, the trap fraction vs resonance strength $G_{30\ell}$ for an initial $\epsilon_0 = 4.62\pi\mu\mathrm{m}$ with various ramping rates. A horizontal line at 2.5% capture efficiency is shown as a line in magenta color. The intercept is the critical resonance strength defined in this paper. Data from Ref. [3] are shown with blue and red boxes with tune ramp rates 8.6×10^{-5} and 1.4×10^{-4} per turn, respectively.

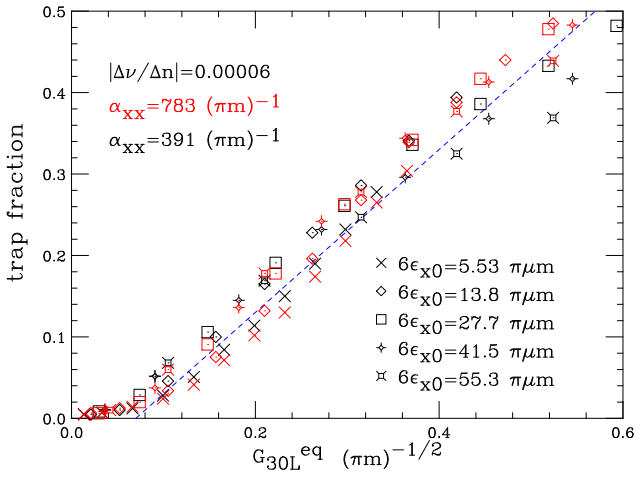

FIG. 20: (Color online) Trap fraction vs the *equivalent* resonance strength for initial emittances $6\epsilon = 5.53, 13.8, 27.7, 41.5,$ and $55.3\ \pi\mu\mathrm{m}$ with tune ramp rate of $d\nu/dn = 6 \times 10^{-5}$ and the nonlinear detuning parameters of $\alpha = 391$ and $783\ (\pi\mathrm{m})^{-1}$ respectively. A single line $f_{\mathrm{trap}} \approx (G_{30\ell}^{\mathrm{eq}} - 0.07)$ drawn through simulation data is to guide the eyes.

duces a 2.5% trap fraction. Such a definition is equivalent to an EGF of 1.2 for the positive detuning case. For a small trap fraction (2.5%), the initial growth mechanism discussed in Sec. V B should work, and a similar power law may be found between the critical resonance strength vs the tune ramping rate and the initial emittance.

Figure VI A shows the power law between the critical resonance strength $\kappa_{30\ell}$ and the tune ramping rate $\Delta\nu/\Delta n$ for 2.5% trap fraction for a number of detuning parameters. A line of $13|d\nu/dn|^{1/2}$ is shown for reference, which agrees well with the scaling law of the negative detuning case.

Increasing the octupole detuning parameter, the slope becomes steeper, and the power law is more like $|d\nu/dn|^{0.62}$ shown in Fig. VI A. For a given beam emittance, a larger α will produce a larger tune spread for the beam, and it will take longer time for the beam to cross the resonance, and effectively more particles will be trapped in resonance islands. Thus a beam with larger detuning parameter can tolerate less resonance strength $G_{30\ell}$, and has a smaller critical resonance strength $\kappa_{30\ell}$.

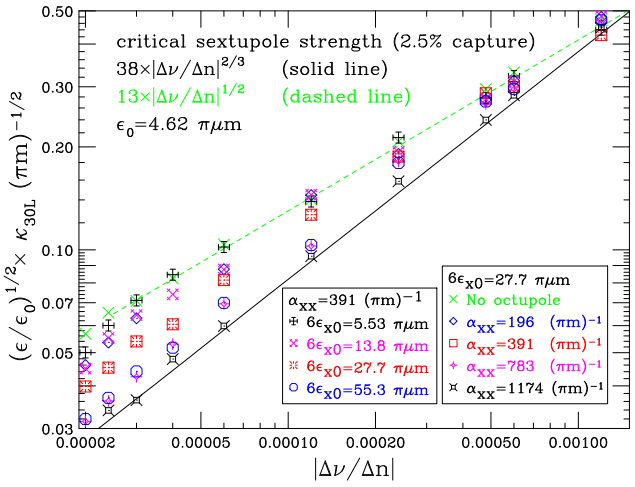

FIG. 21: (Color) The scaled critical resonance strength $\kappa_{30\ell}\sqrt{\epsilon/\epsilon_0}$ vs. tune ramping rate for various detuning coefficients and initial emittances. For cases with different detuning parameters, the initial emittance is fixed at $\epsilon_0 = 4.62\pi\mu m$. For cases with different initial emittances, the detuning parameter is fixed at $\alpha = +391\ (\pi\mathrm{m})^{-1}$. The critical resonance strengths fall within two lines shown in Eqs. (19) and (21).

Figure VI A shows the *scaled* critical resonance strength vs the ramping rate for various beam emittances. The resulting critical resonance strength is

$$\kappa_{30\ell} = 38 \left\{ \frac{4.62\ [\pi\mu\mathrm{m}]}{\epsilon\ [\pi\mu\mathrm{m}]} \right\}^{1/2} \left| \frac{\Delta\nu}{\Delta n} \right|^{2/3} \quad [(\pi\mathrm{m})^{-1/2}], \quad (21)$$

B. Comparison with the scaling law of Ref. [3]

Although Ref. [3] may have different definition of the trapping efficiency, the scaling law should be universal. Based on the "fully adiabatic" parameter of Eq. (27) and Fig. 18 in Ref. [3], the critical resonance strength is

$$G_{\mathrm{ref2}} \le \frac{1}{7^{3/2}} \frac{\left|\frac{\Delta\nu}{\Delta n}\right|}{6\pi 3^{3/2}|\alpha|\epsilon^{3/2}}. \quad (22)$$

This scaling law differs markedly from our critical resonance strength shown in Eqs. (19) and (21) in its power-law dependence on emittance and tune ramp rate. The

$G_{\rm ref2}$ in Ref. [3] shows different dependence on the detuning parameter compared to our results. Besides the extreme difference in the detuning dependency, the dependence on the tune ramping rate is also different. According to the scaling law of Ref. [3], the emittance growth while crossing a resonance will be greatly reduced by increasing the detuning, while according our scaling law, this does not help at all.

VII. CONCLUSIONS

We study the effects of a beam crossing a third-order resonance. The resulting emittance growth and particle capture into the third-order resonance islands are used to characterize the resonance. The phase space evolution depends on the sign of detuning coefficient. If the betatron tune is ramped downward, a negative detuning parameter α will produce emittance growth without particles being captured into resonance islands. We propose a criterion of 20% emittance growth to define the critical resonance strength shown in Fig. 17 and given by Eq. (19), which can be derived from the stationary phase condition on Hamilton's equation of motion. The resulting initial growth scaling law Eq. (18) is linear with respect to the resonance G.

On the other hand, particles will be captured into resonance islands for the positive α case. These captured particles will move outward in phase space as the bare tune is further lowered. For $\alpha > 0$, we propose to use $f_{\rm trap} = 2.5\%$ to define the critical resonance strength, and find that the critical resonance strength vs the tune ramp rate and initial emittance have a simple scaling power-law shown in Fig. VI A. The scaling law falls between Eq. (19) and Eq. (21). Our calculation agrees reasonably well with the experimental data of Ref. [3] shown in Fig. 19. However, our scaling law differs from Eq. (22) based on Ref. [3], which may have a different definition of trapping efficiency or critical resonance strength.

Our method is also applicable to other resonances. We believe that the *stationary phase condition* is a good criterion in solving Hamilton's equation of motion. The scaling law should be applicable to other betatron resonances. For example, the critical resonance of an octupole resonance should scale like $\sim |d\nu/dn|^{1/2}\epsilon^{-1}$ and nearly independent of the nonlinear detuning parameter. Our scaling law can be used in the design of high power accelerators, estimating the emittance growth in cyclotron, and requirement of slow beam extraction using the third-order resonance.

A non-scaling FFAG has recently been commissioned [9]. Our scaling law should be timely for experimental tests. Study of nonlinear resonance scaling law is important for future high power accelerators. Since our scaling law differs markedly from that of Ref. [3], experimental verification would be very timely indeed.

VIII. ACKNOWLEDGMENTS

Work supported by the US DOE under contract DE-FG02-92ER40747, and the NSF under contract NSF PHY-0852368.

[1] P.A. Sturrock, Annals of physics **3**, 113-189 (1958).
[2] A. Chao and M. Month, Nucl. Instru. and Methods, **121**,129 (1974).
[3] M. Aiba, S. Machida, Y. Mori, amd S. Ohnuma, PRSTAB **9**, 084001 (2006).
[4] S.Y. Lee, M. Ball, B. Brabson, D.D. Caussyn, J. Collins, S. Curtis, V. Derenchuk, D. DuPlantis, G. East, M. Ellison, T. Ellison, D. Friesel, B. Hamilton, W.P. Jones, W. Lamble, M.G. Minty, P. Schwandt, T. Sloan, G. Xu, A.W. Chao, S. Tepikian, K.Y. Ng, Phys. Rev. Lett., **67**, 3768 (1991).
[5] See e.g. A.G. Ruggiero, BNL internal report C-A/AP/218, (October 2005); D. Trbojevic, A. G. Ruggiero, E Keil, N. Neskovic, A. Sessler, cyclotron conference, 2004, 19P31 (2004).
[6] S.Y. Lee, Phys. Rev. Lett. **97**, 104801 (2006)
[7] S.Y. Lee, G. Franchetti, I. Hofmann, F. Wang, and L. Yang, New J. Phys. **8**, 291 (2006)
[8] X. Pang, F. Wang, X. Wang, S.Y. Lee, K.Y. Ng, Proceedings of HB2008, p. 118 (2008). http://accelconf.web.cern.ch/AccelConf/HB2008/papers/wga21.pdf
[9] T.R. Edgecock, Proc. of International Particle Accelerator Conference 2010, p. 3593 (2010); http://accelconf.web.cern.ch/AccelConf/IPAC10/papers/thxmh01.pd
[10] see e.g. S. Y. Lee, *Accelerator Physics*, 2nd edition (World Scientific, Singapore, 2004).
[11] R. Cappi and M. Giovannozzi, PRSTAB, **7**, 024001 (2004).
[12] see http://physics.indiana.edu/∼shylee/ap/resonance_3/